

Kinetics of different bioreactor systems with *Acidithiobacillus ferrooxidans* for ferrous iron oxidation

Yavari, Mohsen; Ebrahimi, Sirous; Aghazadeh, Valeh; Ghashghaee, Mohammad

DOI

[10.1007/s11144-019-01660-3](https://doi.org/10.1007/s11144-019-01660-3)

Publication date

2019

Document Version

Final published version

Published in

Reaction Kinetics, Mechanisms and Catalysis

Citation (APA)

Yavari, M., Ebrahimi, S., Aghazadeh, V., & Ghashghaee, M. (2019). Kinetics of different bioreactor systems with *Acidithiobacillus ferrooxidans* for ferrous iron oxidation. *Reaction Kinetics, Mechanisms and Catalysis*, 128(2), 611-627. <https://doi.org/10.1007/s11144-019-01660-3>

Important note

To cite this publication, please use the final published version (if applicable). Please check the document version above.

Copyright

Other than for strictly personal use, it is not permitted to download, forward or distribute the text or part of it, without the consent of the author(s) and/or copyright holder(s), unless the work is under an open content license such as Creative Commons.

Takedown policy

Please contact us and provide details if you believe this document breaches copyrights. We will remove access to the work immediately and investigate your claim.



Kinetics of different bioreactor systems with *Acidithiobacillus ferrooxidans* for ferrous iron oxidation

Mohsen Yavari¹ · Sirous Ebrahimi^{1,4} · Valeh Aghazadeh² ·
Mohammad Ghashghaei³

Received: 16 May 2019 / Accepted: 25 August 2019
© The Author(s) 2019

Abstract

The relative performance of two biofilm-based airlift reactors using different kinds of packing materials and one fixed bed biofilm reactor with a homemade packing material of high specific area ($\sim 1000 \text{ m}^2/\text{m}^3$) was addressed. The bioreactors operated under ferrous iron loading rates in the range of 8–120 mol Fe(II)/ $\text{m}^3 \text{ h}$. *Acidithiobacillus ferrooxidans* cells immobilized in the three bioreactors afforded the reactions for an extended period of 120 days of continuous operation at the dilution rates of 0.2, 0.4, 0.7, 1 and 1.2 h^{-1} . The maximum ferrous iron oxidation rates achieved in this study at a hydraulic residence time of 1.2 h were about 91, 68 and $51 \text{ mol Fe(II)/m}^3 \text{ h}$ for the fixed bed, airlift1, and airlift2 bioreactors. The performance data from the fixed-bed bioreactor offered a higher potential for ferrous iron oxidation because of fast biofilm development, the formation of a thick biofilm, and lower sensitivity to shear, which enhanced the startup time of the bioreactor and the higher reactor productivity. Proper kinetic models were also presented for both the startup period and the steady-state process.

Keywords *Acidithiobacillus ferrooxidans* · Ferrous iron · Airlift bioreactor · Biofilm · Bioleaching · Packed bioreactor

Electronic supplementary material The online version of this article (<https://doi.org/10.1007/s11144-019-01660-3>) contains supplementary material, which is available to authorized users.

✉ Sirous Ebrahimi
S.Ebrahimi@tudelft.nl

¹ Biotechnology Research Centre, Faculty of Chemical Engineering, Sahand University of Technology, Tabriz, Iran

² Faculty of Mining Engineering, Sahand University of Technology, Tabriz, Iran

³ Biobased Monomers and Polymers Division, Iran Polymer and Petrochemical Institute (IPPI), Tehran, Iran

⁴ Gust Researcher, Department of Biotechnology, Faculty of Applied Sciences, Building 58, Vander MAAssweg 9, 2629HZ Delft, The Netherlands

Introduction

Bioleaching is an established technology for the minerals engineering in which the activity of chemolithotrophic bacteria facilitates the extraction of metals from the corresponding (sulfide) ores into the solution [1–4]. Bioleaching is particularly suited to the processing of low-grade refractory ores of, e.g., copper and nickel, and mineral concentrates that cannot be treated by conventional smelting, pressure oxidation, and roasting [5–12]. The underlying mechanism involves the chemical leaching of the mineral by ferric iron, resulting in the formation of ferrous iron, which is subsequently oxidized to ferric iron in the presence of microorganisms [13–15]. Hence, the bioleaching of sulfide minerals consists of two independent chemical and biological sub-processes [13, 16].

The dominance of the cyclic two-step bioleaching mechanism suggests that the biological and chemical sub-processes may be studied and optimized separately toward higher productivity. As two examples, one may note that the chemical oxidation can be enhanced by thermal activation under the optimum surface potential, and the biological stage can be intensified with immobilizing of the ferrous iron-oxidizing bacteria [17, 18].

Process intensification schemes can always be pursued for higher performance of the established technologies throughout the chemical industry [19–27]. Although the bioleaching process is beneficial for climate change mitigation, the slow kinetics of the reactions in this process has to be improved for successful implementation [17], which in turn requires the optimization of the process with respect to the influencing parameters [28]. A critical solution to this problem is the decoupling and optimization of the sub-processes independently [17]. Process decoupling is particularly important in the present case: although high temperature and vigorous mixing favor the reaction kinetics at the chemical stage, they will be detrimental to the lifetime and operation of microorganisms at the biological stage. A third motivation for the decoupling is the fact that fine particles which enhance the leaching rate in a chemical process restrict the effectiveness of the biofilm holdup due to a carryover of the microorganisms. An illustrative diagram of such a decoupling for the case of chalcopyrite is shown in Supplementary Material, Fig. S1, in which the focus of the present study (the biological stage) has been highlighted.

The application of biofilm reactors in the vital biological step can offer several advantages over bioreactors with suspended cells. The immobilization enables reactor operation at high biomass concentrations, leading to high volumetric productivity, the principal factor that affects the cost-effectiveness of relevant industrial processes. Furthermore, in the integrated process for copper extraction from chalcopyrite, the regenerated Fe^{3+} solution is recycled to the chemical oxidation step, where the bacteria might be exposed to high temperature. It is therefore required to prevent the bacteria from entering the first stage. The controlled entrance can be achieved without an external separator in cases where a biofilm-type reactor is employed in the second stage.

Several studies demonstrate the successful immobilization and high rates using the packed bed, fluidized bed, and airlift bioreactors. Various inert carrier

materials have been applied as the support matrix to the biofilm development, including activated carbon, ion-exchange resin [29], glass beads, low-grade ore [30], polystyrene, polyurethane, nickel alloy fiber [31], siliceous stone particles [32], polyurethane foam [33], and poly(vinyl alcohol) cryogel [17]. Among them, plastic media are the most frequently used materials as the biofilm support in the biofilm-based bioreactors.

The ability of bacterium *Acidithiobacillus ferrooxidans* to form biofilms on different carrier materials is quite promising for increasing the iron(II) biooxidation rate and the development of a high-performance compact bioreactor system for a full-scale implementation of metal leaching technologies as well as the purification of gases containing sulfur compounds and acid mine drainage treatment [34–37]. However, most of the investigations on the biofilm-based ferrous iron oxidation systems have been reported with different bioreactors at different scales. It is, therefore, difficult to compare the results of different studies, and they do not provide the quantitative data required for the design of a large-scale reactor for the bioleaching of the sulfide mineral; meanwhile, the disadvantages are not often recognized and are rarely made available to third parties.

In this work, the kinetics of the biological oxidation of ferrous iron was investigated using *Acidithiobacillus ferrooxidans* bacteria in three continuously operated biofilm-based bioreactors. Two reactors were based on an internal loop airlift system using polystyrene (PS) granules and polyvinyl chloride (PVC) particles as the carrier materials, and the third one was a fixed bed reactor with a homemade, high specific area, polyethylene (PE) packing for the biofilm formation. As far as the authors are aware, the present report is the first in addressing the performance of such different bioreactor systems at identical conditions. Moreover, the volume of the reactors was designed to be larger than most of the previous works to approach large-scale insights into the process at hand. Meanwhile, the oxidation kinetics is addressed for both the startup period and the steady-state operation.

Materials and methods

Reactor and operation conditions

Three laboratory-scale biofilm bioreactors were used for the experiments (two airlifts and one fixed bed systems). For the fixed-bed bioreactor, a column (reactor) with a liquid volume of 1.5 L with homemade PE packing with the specific area of $\sim 1000 \text{ m}^2/\text{m}^3$ was used. For the airlift systems, two bioreactors with the sizes of 1.5 L were employed, which contained small PS and PVC particles as the carrier materials. The vertical columns of the reactors were made of double-glazing glass with a pathway for the heating/cooling liquid to fix the temperature at $31 \pm 1 \text{ }^\circ\text{C}$. The pH and redox potential in the reactors were continuously monitored. The pH of the liquid in the reactors was measured, but not controlled. However, they were maintained at the required pH by controlling the pH of the feed influent to the reactor using a 2 M sulfuric acid solution. The pH in the feed solution was set to 1.4 ± 0.1 . The resulting pH of the liquid in the reactor was in the range of 1.4–1.6. The airflow

rate was set to 6 ± 1 L/min utilizing a rotameter. Before entering the reactor, the air was led through a humidifier to minimize evaporation. The air was sparged with a silicon tube sparger.

PS and PVC particles with a density of 1.027 kg/L and the mean diameter of 1 mm were used in the airlift reactors. For both cases, the concentrations of particles were 5% of the total volume. Under these conditions, the carrier materials have been suspended in the airlift reactors. Before running the systems, the particles were treated with 0.1 N H_2SO_4 solution for 2 days and washed until neutral to remove the acid soluble salts. For the fixed bed system, a packing material with the specific surface of $1000 \text{ m}^2/\text{m}^3$ and the density of 0.814 kg/L was used, and the treatment was the same as in the other reactors.

Microorganism and media

A defined pure culture of *A. ferrooxidans* (PTCC1646) was used as inoculums, obtained from Iranian Microbial Culture Collection in Tehran, Iran. Further details on the microbial identification and study of the competition between the two main iron-oxidizing microorganisms, *Acidithiobacillus ferrooxidans* and *Leptospirillum ferrooxidans*, using the fluorescence in situ hybridization (FISH) technique, can be found in our previous study [1]. The composition (in g/L) of the medium for an influent Fe^{2+} concentration of 33.3 g/L with $\text{FeSO}_4 \cdot 7\text{H}_2\text{O}$ was as follows: $(\text{NH}_4)_2\text{SO}_4$, 0.3; K_2HPO_4 , 0.3; $\text{MgSO}_4 \cdot 7\text{H}_2\text{O}$, 0.3. The pH value was set with the 1 M H_2SO_4 (Merck) solution to the required levels. In the subsequent steps, the concentrations of the medium were doubled and tripled to check the effects of suspended and fixed biofilm configurations on the performance of the systems.

Analytical procedures

On-line redox-potential measurements were used to identify the oxidation performance of the reactor. The dissolved oxygen (DO) was measured discontinuously as the continuous measurement of DO was not convenient due to the precipitation and low pH effects. Total iron and Fe^{2+} concentrations were determined by the colorimetric ortho-phenanthroline method, following the standard method D1068 from the American Society for Testing and Materials (ASTM). At low ferrous iron concentrations, the background color of the ferric iron in the sample caused an error in the colorimetric measurement; therefore, these measurements had to be corrected by measuring the absorbance of a blank sample into which no ortho-phenanthroline had been introduced.

Kinetic modeling

The logistic equation has been widely employed to model both batch and continuous cell growth kinetics in biooxidation and other biological systems [38–51]. Here, we used the extended Prout–Tompkins model [52–55] as a generalized logistic equation as follows for the startup kinetics.

$$x = x_m \left[1 - 1 / \left(1 + \frac{\omega}{e^{b(t-c)}} \right)^{1/\omega} \right] \quad (1)$$

Here x is the time-dependent conversion [%], x_m is the maximum conversion [%], t represents the time on stream [h], b is the negative of the conventional reaction rate constant [h^{-1}], c represents an arbitrary shift in time [h], and ω is a shape parameter [-]. When appropriately differentiated, this equation becomes:

$$\frac{dx}{dt} = x_m \left(-\frac{b}{\omega} \left(1 - \frac{x}{x_m} \right) \left[1 - \left(1 - \frac{x}{x_m} \right)^\omega \right] \right) \quad (2)$$

For a mixed-flow (chemostat) bioreactor, Eq. 2 can be reformulated as follows:

$$x = x_m \left(-\frac{bt}{\omega} \left(1 - \frac{x}{x_m} \right) \left[1 - \left(1 - \frac{x}{x_m} \right)^\omega \right] \right) \quad (3)$$

For the steady-state conditions, we employed an equation similar to the Jones–Kelly model [56]:

$$-r_{\text{Fe}^{2+}} = \frac{k[\text{Fe}^{2+}]}{[\text{Fe}^{2+}] + K_m \left(1 + \frac{[\text{Fe}^{3+}]}{K_i} \right)} \quad (4)$$

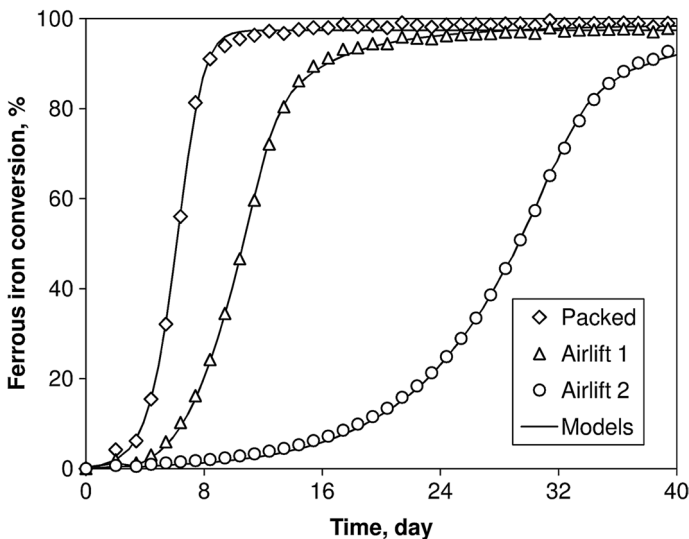


Fig. 1 Time-dependent evolution of the ferrous iron conversion in the three packed and airlift bioreactors during the startup period at 31 ± 1 °C with immobilized *A. ferrooxidans*; the Fe(II) feed concentration was constant at 0.04 M, the airflow rate was 6 ± 1 L/min, and the pH of the feedstock was set to 1.4 ± 0.1 . The concentration data were estimated to remain accurate within $\pm 1.3\%$

Here $-r_{\text{Fe}^{2+}}$ is the overall ferrous iron oxidation rate [mol/(L h)], $[\text{Fe}^{2+}]$ is the concentration of ferrous iron [mol/L], k is the maximum oxidation rate [mol/(L h)], K_m is the substrate affinity constant [mol/L], and K_i denotes the ferric product inhibition constant [–]. It is noteworthy that Eq. 4 is written in terms of the reaction volume and, therefore, we have:

$$-r_{\text{Fe}^{2+}} = q_{\text{Fe}^{2+}}[X] \text{ and } k = q_{\text{max}}[X] \quad (5)$$

Here $q_{\text{Fe}^{2+}}$ is the bacterial specific ferrous-iron utilization rate [mol/(mol X·h)], q_{max} is the maximum bacterial specific utilization rate [mol/(mol X h)], and $[X]$ represents the cell concentration [mol X/L].

Equation 4 was applied to the reaction rate data from airlift and packed bed bioreactors with appropriate mass balance equations. Finally, the best set of kinetic parameters was obtained by the minimization of the sum of squared errors of the model predictions as the objective function (OF):

$$\text{OF} = \sum \left([\text{Fe}^{2+}]^{\text{exp}} - [\text{Fe}^{2+}]^{\text{mod}} \right) \quad (6)$$

Here the superscripts exp and mod refer to the experimental and model values of time-dependent concentration.

Results and discussion

Bioreactors startup performance and biofilm formation

During the startup period, the reactors were filled with a 0.04 M ferrous solution and were inoculated with *A. ferrooxidans* at an initial dry weight (DW) concentration of 10 mg DW/L. Initially, the bioreactors were operated in batch mode with a constant aeration rate of 5 L/min, corresponding to a superficial air velocity of 0.06 m/s, to keep high DO concentrations in the bulk liquid phase. Following the accomplishment of 95% conversion of ferrous iron, continuous feeding was initiated with the ferrous iron concentration of 0.04 M. The residence time in all reactors was adjusted to 5 h, which is much shorter than the residence time corresponding to the critical (washout) dilution rate of *A. ferrooxidans* to stimulate the biofilm formation (16 h). The time courses of ferrous iron conversions during this period (over 40 days of operation) for all three reactors are illustrated in Fig. 1.

Table 1 Kinetic constants of the startup period obtained from the fit of the reaction rate data to the extended Prout–Tompkins model

Reactor	ω	b	c	R^2
Packed	0.5786	–0.0383	150.2088	0.9984
Airlift 1	–0.6120	–0.0047	–	0.9996
Airlift 2	–0.7570	–0.0016	–	0.9996

Units: b (h^{-1}), c (h), ω is dimensionless

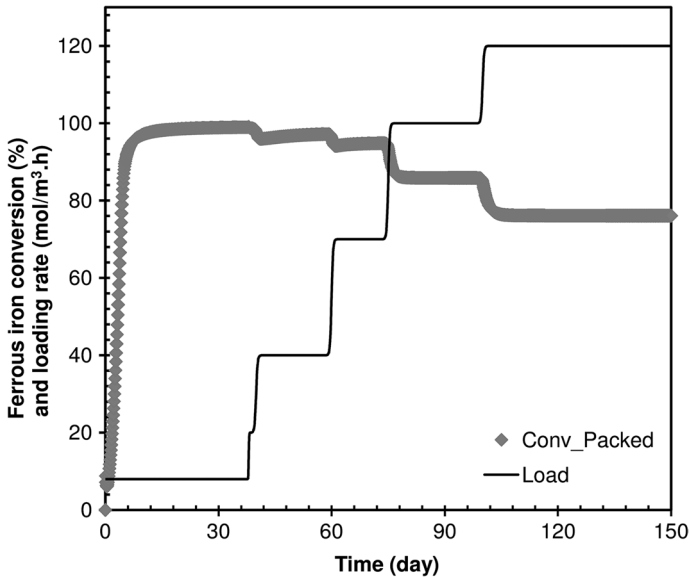


Fig. 2 Changes in the ferrous iron loading affected the ferrous iron conversion as a function of time in the packed-bed bioreactor at 31 ± 1 °C with immobilized *A. ferrooxidans*; the Fe(II) feed concentration was constant at 0.1 M after day 40, the airflow rate was 6 ± 1 L/min, and the pH of the feedstock was set to 1.4 ± 0.1 . The concentration data were estimated to remain accurate within $\pm 1.3\%$

During this transient period, the ferrous iron loading rate of all reactors was kept constant at $8 \text{ mol/m}^3 \text{ h}$. Fig. 1 shows that the ferrous iron conversion in all reactors increased as the biomass concentration started to increase because of the biofilm formation. The sharp increase in the ferrous iron conversion in the packed-bed reactor can be postulated to be a consequence of low shear and the establishment of thin ferric iron precipitation on the surface of the carrier materials, which stimulate the biofilm development. The batch tests at the end of the startup period revealed that more than 95% of the biological activity in all reactors occurred in the immobilized biomass, which confirmed the active biofilm formation in all reactors.

The startup kinetic parameters are shown in Table 1. Ideal mixed-flow and plug-flow reactor models were assumed for the airlift and fixed-bed bioreactor systems. As indicated by the coefficients of multiple determination and the fits to the experimental data points (Fig. 1), the generalized logistic equation has given an excellent fit to both airlift and packed bed sets of data. Fig. 1 shows that the transient behavior of the microorganisms is highly dependent on the bioreactor system at hand.

Effect of loading rate in different bioreactors

Influence of the ferrous iron loading rate on the substrate uptake rate and conversion in different bioreactors was studied in detail by a stepwise augmenting of the feeding

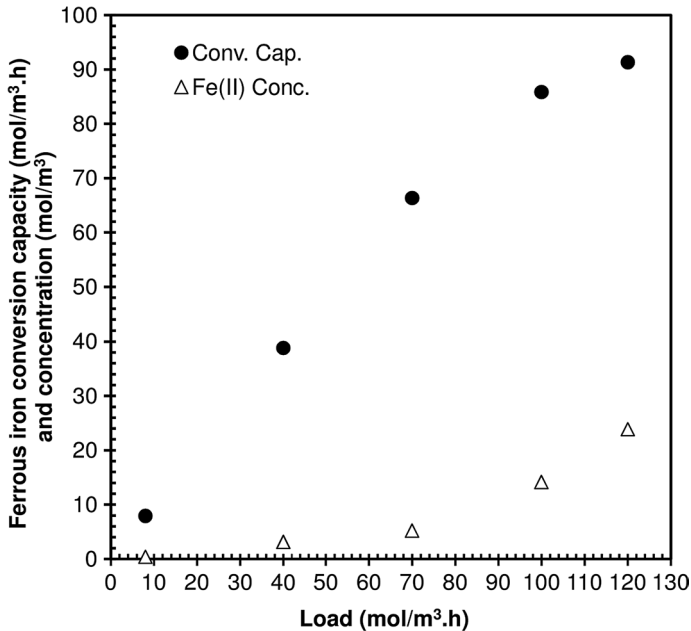


Fig. 3 Steady-state ferrous iron oxidation rate and the residual ferrous iron concentration as a function of ferrous iron loading rate in the fixed-bed biofilm bioreactor at 31 ± 1 °C with immobilized *A. ferrooxidans*; the Fe(II) feed concentration was constant at 0.1 M after day 40, the airflow rate was 6 ± 1 L/min, and the pH of the feedstock was set to 1.4 ± 0.1 . The concentration data were estimated to remain accurate within $\pm 1.3\%$

rate. The inlet ferrous iron concentration was 0.04 M during the startup period, which was increased to 0.1 M on day 40 and the entire operation period afterward was kept constant at 0.1 M. The operational feeding flow rate was increased stepwise from 0.6 to 36 L/h, corresponding to the ferrous iron loadings of 8 to 120 mol/m³·h or the dilution rates of 0.2, 0.4, 0.7, 1 and 1.2 h⁻¹. The bioreactor was operated at each loading rate for at least five residence time intervals before the final steady-state was assumed. Furthermore, the steady-state in the conversion was assumed only once the redox potential and the pH in the bioreactor became constant.

The results of the experiments for the packed reactor are shown in Fig. 2, in which the variation of the ferrous iron conversion with time due to the changes in the ferrous iron loading rate is presented. The steady-state conversion of ferrous iron was 99% at the loading rate of 8 mol/m³·h and was decreased to 97, 94, 85 and 76% as the loading rate was increased to 40, 70, 100 and 120 mol/m³ h.

Fig. 3 shows the corresponding steady-state ferrous iron oxidation rate and the residual ferrous iron concentration as a function of loading rate. At low loading rates of < 70 mol Fe(II)/m³ h, the ferrous iron oxidation rate increased linearly with the increase in the loading rate, while the conversion rate of Fe²⁺ to Fe³⁺ remained almost constant at a value above 95%. At high loading rates, the biomass concentration limited the increase in the ferrous iron oxidation rate. As a result, the outlet ferrous iron concentration increased. Notably, when the loading rate was further

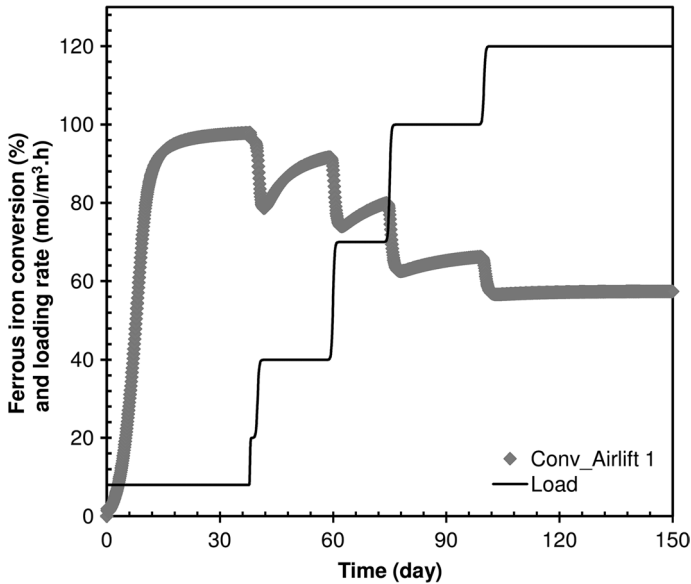


Fig. 4 Changes in the ferrous iron loading led to corresponding changes in the ferrous iron conversion as a function of time in the airlift bioreactor1 at 31 ± 1 °C with immobilized *A. ferrooxidans*; the Fe(II) feed concentration was constant at 0.1 M after day 40, the airflow rate was 6 ± 1 L/min, and the pH of the feedstock was set to 1.4 ± 0.1 . The concentration data were estimated to remain accurate within $\pm 1.3\%$

increased to 100 and 120 mol $\text{Fe}^{2+}/\text{m}^3$ h, the ferrous iron conversion efficiency was decreased significantly to 71 and 63%.

The results of the experiments with the airlift bioreactor 1 are shown in Fig. 4, in which the variation of the ferrous iron conversion with time due to the change in the ferrous iron loading rate is presented. The steady-state conversion of the ferrous iron was 98% at the loading rate of 8 mol/ m^3 ·h, and it was decreased to 91, 79, 66 and 57% as the loading rate was increased to 40, 70, 100 and 120 mol/ m^3 h.

Fig. 5 shows the corresponding values of the obtained steady-state ferrous iron oxidation rate and the residual ferrous iron concentration as a function of loading rate. At low loading rates of < 40 mol $\text{Fe}^{2+}/\text{m}^3$ h, the ferrous oxidation rate increased linearly with increasing of the loading rate, while the rate of conversion of Fe^{2+} to Fe^{3+} became almost constant at loading values above 40 mol $\text{Fe}^{2+}/\text{m}^3$ h. At high loading rates, the biomass concentration limited further increase in the ferrous oxidation rate; as a result, the conversion of ferrous iron was hampered. When the ferrous iron loading rate was increased from 70 to 100 and 120 mol $\text{Fe}^{2+}/\text{m}^3$ h, the ferrous iron conversion efficiency was decreased remarkably from 66 to 54 and 47%.

The results of the experiments with the airlift bioreactor 2 are shown in Fig. 6, in which the variation of the ferrous iron conversion with time due to the change in the ferrous iron loading rate is presented. The steady-state conversion of the ferrous iron approached ca. 96% at the loading rate of 8 mol/ m^3 ·h, which was further decreased to 92, 71, 51 and 43% as the loading rate was increased stepwise to 40, 70, 100 and 120 mol/ m^3 h.

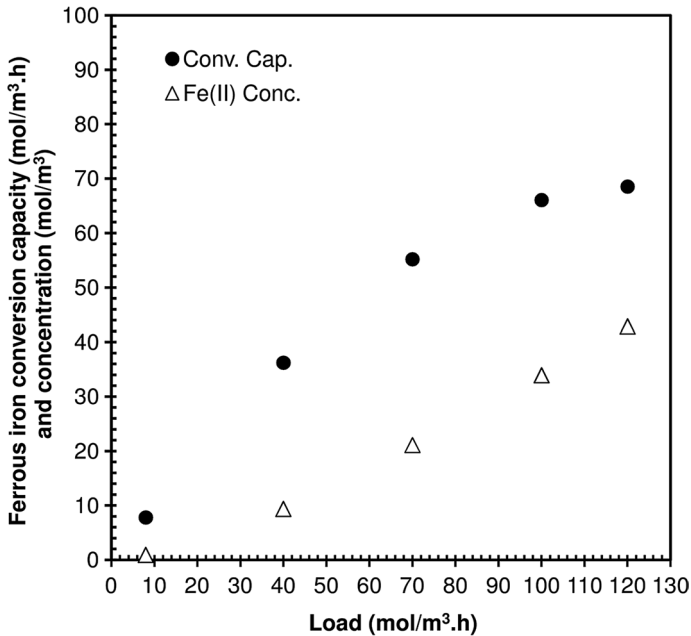


Fig. 5 Steady-state ferrous iron oxidation rate and the residual ferrous iron concentration as a function of ferrous iron loading rate in the airlift bioreactor1 at 31 ± 1 °C with immobilized *A. ferrooxidans*; the Fe(II) feed concentration was constant at 0.1 M after day 40, the airflow rate was 6 ± 1 L/min, and the pH of the feedstock was set to 1.4 ± 0.1 . The concentration data were estimated to remain accurate within $\pm 1.3\%$

Fig. 7 shows the corresponding values of the obtained steady-state ferrous iron oxidation rate and the residual ferrous iron concentration as a function of loading rate. From Fig. 7, two regimes could be distinguished. At low loading rates, particularly at < 40 mol Fe²⁺/m³ h, the ferrous oxidation rate increased linearly with increasing loading rate, while the rate of conversion of Fe²⁺ to Fe³⁺ remained almost constant at a value around 90%. At high loading rates, the biomass concentration limited the increase in ferrous iron oxidation rate, and thus the conversion of ferrous iron was hampered. When the ferrous iron loading rate was increased from 70 to 100 and 120 mol Fe²⁺/m³ h, the ferrous iron conversion efficiency was decreased remarkably from 71 to 51 and 43%.

Kinetic modeling of bioreactors under steady-state conditions

As mentioned previously, the Jones–Kelly model was applied to the packed-bed and moving-bed bioreactors, assuming that they operate as ideal plug-flow and mixed-flow reactors. Fig. 8 shows the parity plot for the goodness-of-fit of the model equations to the experimental rate data. Fair correspondence has been obtained between the models and the experimental data. Table 2 further shows the obtained kinetic parameters. Although the inhibition constants have been mainly the same for all

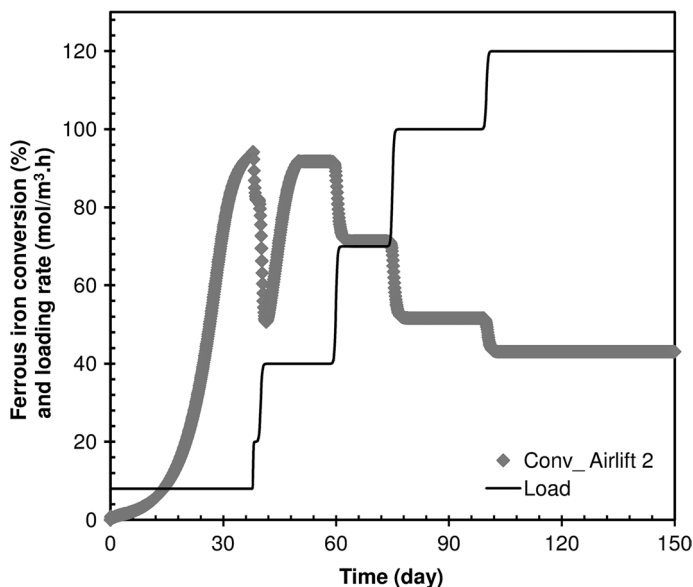


Fig. 6 Changes in the ferrous iron loading affect the ferrous iron conversion as a function of time in the airlift bioreactor2 at 31 ± 1 °C with immobilized *A. ferrooxidans*; the Fe(II) feed concentration was constant at 0.1 M after day 40, the airflow rate was 6 ± 1 L/min, and the pH of the feedstock was set to 1.4 ± 0.1 . The concentration data were estimated to remain accurate within $\pm 1.3\%$

three bioreactor systems, the relative magnitude of maximum ferrous iron utilization constant to substrate affinity varied in the order of airlift 1 ~ airlift 2 \ll packed, which suggests the higher potential of the packed-bed bioreactor compared to the airlift counterparts investigated here. The faster drop in the Fe^{2+} concentration with the former bioreactor, as shown in Fig. 9, is another presentation of this privilege.

Advancement and concluding remarks

Finally, we may compare the results with those published previously. Table S1 contains the optimum values obtained in the present study with those reported previously with different bioreactor systems. A reaction rate of 3.8 g/L h was accomplished using the airlift reactor with the PVC support matrix. An even higher maximum oxidation rate (5.5 g/L h) has been achieved using the packed-bed bioreactor with the PE packing at the pH level of 1.4, which is obviously higher than the highest value (3.3 g/L h) reported previously with an ion-exchange resin within the same type of reactor at comparable pH values of 1.3–1.5. This difference confirms that improvement has been made in the efficiency of the biooxidation of the ferrous ion using a more suitable packing material compared to ion-exchange resin or PVA, thus taking one step forward in the field from a practical point of view. Notably, the packing used in the present study for the fixed-bed operation is capable of being scaled-up over long-range

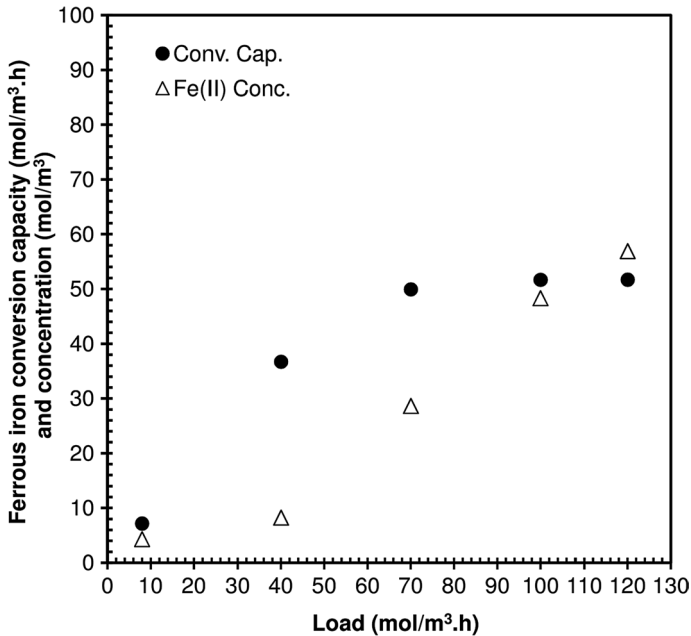


Fig. 7 Steady-state ferrous iron oxidation rate and the residual ferrous iron concentration as a function of ferrous iron loading rate in the airlift bioreactor2 at 31 ± 1 °C with immobilized *A. ferrooxidans*; the Fe(II) feed concentration was constant at 0.1 M after day 40, the airflow rate was 6 ± 1 L/min, and the pH of the feedstock was set to 1.4 ± 0.1 . The concentration data were estimated to remain accurate within $\pm 1.3\%$

implementations when compared to the earlier systems using, e.g., glass beads as the packing. It may be conceived that the employed microorganism has been effectively trapped in the small pores of the packing, thus forming an ideal biofilm inside the fixed-bed bioreactor. The observed superior performance of the packed-bed bioreactor would be particularly impressive, taking into account that the oxygen transfer capacity of a packed bed reactor is expected to be lower than in an airlift reactor [1].

Conclusion

This article dealt with the relative performance of two biofilm-based airlift reactors and one fixed bed biofilm reactor in the bioleaching of sulfide mineral for ferrous ion oxidation. Fe(II) loading rates in the range of 8–120 mol/m³.h were applied with *Acidithiobacillus ferrooxidans* cells immobilized on different packing materials in the three bioreactors. Successful continuous operation of the bioreactors was established over an extended period of 120 days. Two different (beginning and ending) regions concerning the loading rate were identified in most of the cases for the steady-state ferrous iron oxidation rate and ferrous iron concentration so that the operation reached almost a plateau after the conversion

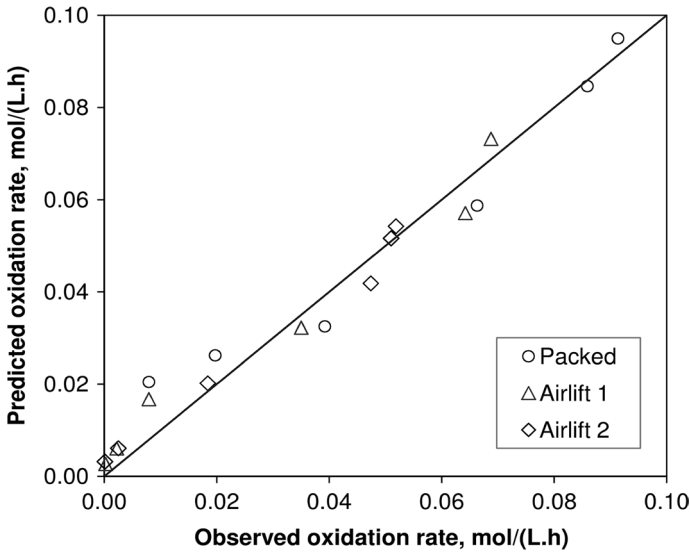


Fig. 8 Parity plot for the quality of kinetic modeling of steady-state ferrous iron oxidation in the three bioreactors at 31 ± 1 °C with immobilized *A. ferrooxidans*; the Fe(II) feed concentration was constant at 0.1 M, the airflow rate was 6 ± 1 L/min, and the pH of the feedstock was set to 1.4 ± 0.1 . The concentration data were estimated to remain accurate within $\pm 1.3\%$

Table 2 Kinetic constants from the fit of the reaction rate data to the Jones–Kelly model

Reactor	k	K_m	K_i	R^2
Packed	0.1151	0.0051	17.5836	0.9374
Airlift 1	0.4559	0.2227	17.5835	0.9580
Airlift 2	0.0762	0.0229	17.5837	0.9761

Units: k [mol/(L h)], K_m (mol/L), K_i is dimensionless

rate of 95%. The maximum oxidation rates obtained in the present work at the hydraulic residence time of 1.2 h were 91, 68 and 51 mol/m³ h within the fixed bed, airlift1, and airlift2 bioreactors. On the other hand, the conversion of ferrous iron in the fixed bed bioreactor met 95% within 10 days in the startup period while the corresponding time in the airlift2 bioreactor exceeded 40 days. Hence, the fixed bed bioreactor was regarded superior to the airlift bioreactors at the same operating conditions owing mainly to fast biofilm development, the formation of a thick biofilm, and lower sensitivity to shear, which altogether extend the startup time and productivity of the bioreactor. Finally, the kinetics of the startup period was described satisfactorily using the generalized logistic equation. The steady-state kinetics of the three bioreactor systems was fairly described by the Jones–Kelly model with the assumptions of ideal mixed-flow and plug-flow reactors.

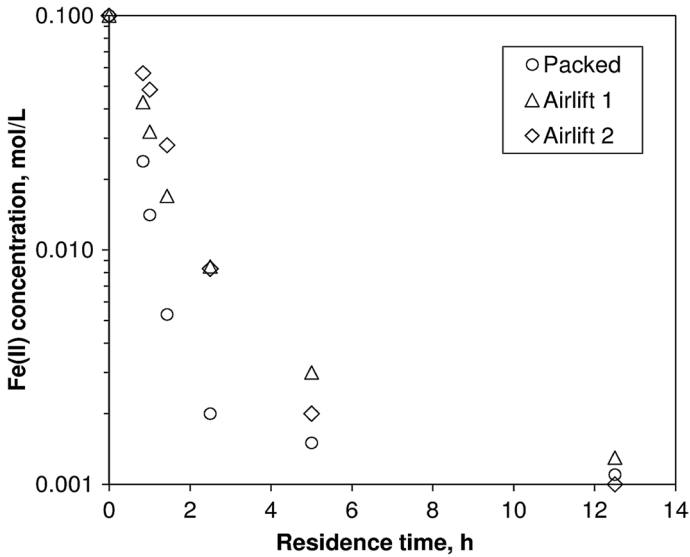


Fig. 9 Variations of ferrous iron concentration with residence time (the inverse of dilution rate) for the biooxidation in the three bioreactors at 31 ± 1 °C with immobilized *A. ferrooxidans*; the Fe(II) feed concentration was constant at 0.1 M, the airflow rate was 6 ± 1 L/min, and the pH of the feedstock was set to 1.4 ± 0.1 . The concentration data were estimated to remain accurate within $\pm 1.3\%$

Funding This research did not receive any specific grant from funding agencies in the public, commercial, or not-for-profit sectors.

Compliance with ethical standards

Conflicts of interest The authors declare that they have no conflicts of interest.

Open Access This article is distributed under the terms of the Creative Commons Attribution 4.0 International License (<http://creativecommons.org/licenses/by/4.0/>), which permits unrestricted use, distribution, and reproduction in any medium, provided you give appropriate credit to the original author(s) and the source, provide a link to the Creative Commons license, and indicate if changes were made.

References

1. Ebrahimi S, Fernandez Morales FJ, Kleerebezem R, Heijnen JJ, van Loosdrecht MC (2005) High-rate acidophilic ferrous iron oxidation in a biofilm airlift reactor and the role of the carrier material. *Biotechnol Bioeng* 90(4):462–472. <https://doi.org/10.1002/bit.20448>
2. Gilbertson BP (2000) Creating value through innovation: biotechnology in mining. *Miner Process Extr Metall* 109(2):61–67. <https://doi.org/10.1179/mpm.2000.109.2.61>
3. Jonglertjunya W (2003) Biorecovery of chalcocopyrite. The University of Birmingham, Birmingham
4. Konishi Y, Asai S, Tokushige M, Suzuki T (1999) Kinetics of the bioleaching of chalcocopyrite concentrate by acidophilic thermophile acidianus brierleyi. *Biotechnol Prog* 15(4):681–688. <https://doi.org/10.1021/bp9900662>

5. Halinen A-K, Rahunen N, Kaksonen AH, Puhakka JA (2009) Heap bioleaching of a complex sulfide ore: part I: effect of pH on metal extraction and microbial composition in pH controlled columns. *Hydrometallurgy* 98(1–2):92–100. <https://doi.org/10.1016/j.hydromet.2009.04.005>
6. Brierley JA, Brierley CL (2001) Present and future commercial applications of biohydrometallurgy. *Hydrometallurgy* 59(2–3):233–239. [https://doi.org/10.1016/S0304-386X\(00\)00162-6](https://doi.org/10.1016/S0304-386X(00)00162-6)
7. Morin D, Lips A, Pinches T, Huisman J, Frias C, Norberg A, Forssberg E (2006) BioMinE—integrated project for the development of biotechnology for metal-bearing materials in Europe. *Hydrometallurgy* 83(1–4):69–76. <https://doi.org/10.1016/j.hydromet.2006.03.047>
8. Watling HR (2006) The bioleaching of sulphide minerals with emphasis on copper sulphides: a review. *Hydrometallurgy* 84(1–2):81–108. <https://doi.org/10.1016/j.hydromet.2006.05.001>
9. Barrett J (1993) Metal extraction by bacterial oxidation of minerals. Ellis Horwood, New York
10. Miller PC, Rhodes MK, Winby R, Pinches A, van Staden P (1999) Commercialization of bioleaching for base-metal extraction. *Min Metall Explor* 16:42–50. <https://doi.org/10.1007/bf03403233>
11. Halinen A-K, Rahunen N, Kaksonen AH, Puhakka JA (2009) Heap bioleaching of a complex sulfide ore: part II. Effect of temperature on base metal extraction and bacterial compositions. *Hydrometallurgy* 98(1):101–107. <https://doi.org/10.1016/j.hydromet.2009.04.004>
12. Dew DW, Van Buuren C, McEwan K, Bowker C (2000) Bioleaching of base metal sulphide concentrates: a comparison of high and low temperature bioleaching. *J S Afr Inst Min Metall* 100:409–414
13. Bircumshaw L, Changunda K, Hansford GS, Rawatlal R (2006) Development of a mathematical model for continuous tank bioleaching. *J S Afr Inst Min Metall* 106:277–282
14. Rawlings DE, Tributsh H, Hansford GS (1999) Reasons why ‘Leptospirillum’-like species rather than *Thiobacillus ferrooxidans* are the dominant iron-oxidizing bacteria in many commercial processes for the biooxidation of pyrite and related ores. *Microbiology* 145(Pt 1):5–13. <https://doi.org/10.1099/13500872-145-1-5>
15. Battaglia-Brunet F, d’Hugues P, Cabral T, Cezac P, Garcia JL, Morin D (1998) The mutual effect of mixed thiobacilli and leptospirilli populations on pyrite bioleaching. *Miner Eng* 11(2):195–205. [https://doi.org/10.1016/S0892-6875\(97\)00151-9](https://doi.org/10.1016/S0892-6875(97)00151-9)
16. Boon M, Heijnen JJ (1998) Chemical oxidation kinetics of pyrite in bioleaching processes. *Hydrometallurgy* 48(1):27–41. [https://doi.org/10.1016/S0304-386X\(97\)00072-8](https://doi.org/10.1016/S0304-386X(97)00072-8)
17. Long ZE, Huang Y, Cai Z, Cong W, Ouyang F (2003) Biooxidation of ferrous iron by immobilized *Acidithiobacillus ferrooxidans* in poly(vinyl alcohol) cryogel carriers. *Biotechnol Lett* 25(3):245–249
18. Breed GS, Dempers CJN, Hansford GS (2000) Studies on the bioleaching of refractory concentrates. *J S Afr Inst Min Metall* 100:389–398
19. Ghashghae M, Shirvani S, Kegnaes S (2019) Steam catalytic cracking of fuel oil over a novel composite nanocatalyst: characterization, kinetics and comparative perspective. *J Anal Appl Pyrol* 138:281–293. <https://doi.org/10.1016/j.jaap.2019.01.010>
20. Ghashghae M, Shirvani S (2019) Catalytic transformation of ethylene to propylene and butene over an acidic Ca-incorporated composite nanocatalyst. *Appl Catal A* 569:20–27. <https://doi.org/10.1016/j.apcata.2018.10.017>
21. Ghashghae M (2018) Thorough assessment of delayed coking correlations against literature data: development of improved alternative models. *React Kinet Mech Cat* 126(1):83–102. <https://doi.org/10.1007/s11144-018-1467-0>
22. Ghashghae M (2018) Heterogeneous catalysts for gas-phase conversion of ethylene to higher olefins. *Rev Chem Eng* 34(5):595–655. <https://doi.org/10.1515/revce-2017-0003>
23. Ghashghae M, Shirvani S (2018) Two-step thermal cracking of an extra-heavy fuel oil: experimental evaluation, characterization, and kinetics. *Ind Eng Chem Res* 57(22):7421–7430. <https://doi.org/10.1021/acs.iecr.8b00819>
24. Shirvani S, Ghashghae M (2018) Combined effect of nanoporous diluent and steam on catalytic upgrading of fuel oil to olefins and fuels over USY catalyst. *Petrol Sci Technol* 36(11):750–755. <https://doi.org/10.1080/10916466.2018.1445104>
25. Sadjadi S, Farzaneh V, Shirvani S, Ghashghae M (2017) Preparation of Cu-MgO catalysts with different copper precursors and precipitating agents for the vapor-phase hydrogenation of furfural. *Korean J Chem Eng* 34(3):692–700. <https://doi.org/10.1007/s11814-016-0344-7>
26. Ghashghae M, Shirvani S, Ghambarian M, Eidi A (2019) Two-stage thermocatalytic upgrading of fuel oil to olefins and fuels over a nanoporous hierarchical acidic catalyst. *Pet Sci Technol* 37(16):1910–1916. <https://doi.org/10.1080/10916466.2018.1463257>

27. Karimzadeh R, Ghashghaee M (2008) Design of a flexible pilot plant reactor for the steam cracking process. *Chem Eng Technol* 31(2):278–286. <https://doi.org/10.1002/ceat.200700326>
28. Breed AW, Dempers CJN, Hansford GS (2000) Studies on the bioleaching of refractory concentrates. *J South Afr Inst Min Metall* 100:389–398
29. Grishin SI, Tuovinen OH (1988) Fast kinetics of Fe^{2+} oxidation in packed-bed reactors. *Appl Environ Microbiol* 54(12):3092–3100
30. Carranza F, Garcia MJ (1990) Kinetic comparison of support materials in the bacterial ferrous iron oxidation in packed-bed columns. *Biorecovery* 2(1):15–27
31. Gomez JM, Cantero D, Webb C (2000) Immobilisation of *Thiobacillus ferrooxidans* cells on nickel alloy fibre for ferrous sulfate oxidation. *Appl Microbiol Biotechnol* 54(3):335–340
32. Mazuelos A, Romero R, Palencia I, Iglesias N, Carranza F (1999) Continuous ferrous iron biooxidation in flooded packed bed reactors. *Miner Eng* 12(5):559–564. [https://doi.org/10.1016/S0892-6875\(99\)00037-0](https://doi.org/10.1016/S0892-6875(99)00037-0)
33. Armentia H, Webb C (1992) Ferrous sulphate oxidation using *Thiobacillus ferrooxidans* cells immobilised in polyurethane foam support particles. *Appl Microbiol Biotechnol* 36(5):697–700. <https://doi.org/10.1007/BF00183252>
34. Kai T, Nagano T, Fukumoto T, Nakajima M, Takahashi T (2007) Autotrophic growth of *Acidithiobacillus ferrooxidans* by oxidation of molecular hydrogen using a gas–liquid contactor. *Bioreactor Technol* 98(2):460–464. <https://doi.org/10.1016/j.biortech.2006.01.003>
35. Malhotra S, Tankhiwale AS, Rajvaidya AS, Pandey RA (2002) Optimal conditions for bio-oxidation of ferrous ions to ferric ions using *Thiobacillus ferrooxidans*. *Bioresour Technol* 85(3):225–234. [https://doi.org/10.1016/S0960-8524\(02\)00148-7](https://doi.org/10.1016/S0960-8524(02)00148-7)
36. Pagella C, Perego P, Zilli M (1996) Biotechnological H_2S gas treatment with *Thiobacillus ferrooxidans*. *Chem Eng Technol* 19(1):79–88. <https://doi.org/10.1002/ceat.270190113>
37. Halfmeier H, Schäfer-Treffenfeldt W, Reuss M (1993) Potential of *Thiobacillus ferrooxidans* for waste gas purification Part 2 Increase in continuous ferrous iron oxidation kinetics using immobilized cells. *Appl Microbiol Biotechnol* 40(4):582–587. <https://doi.org/10.1007/bf00175751>
38. Hansford GS, Chapman JT (1992) Batch and continuous biooxidation kinetics of a refractory gold-bearing pyrite concentrate. *Miner Eng* 5(6):597–612. [https://doi.org/10.1016/0892-6875\(92\)90057-G](https://doi.org/10.1016/0892-6875(92)90057-G)
39. Germec M, Turhan I, Karhan M, Demirci A (2019) Kinetic modeling and techno-economic feasibility of ethanol production from carob extract based medium in biofilm reactor. *Appl Sci* 9(10):2121
40. Shonkwiler RW, Herod J (2009) *Mathematical biology: an introduction with maple and Matlab*, 2nd edn. Springer, Dordrecht. <https://doi.org/10.1007/978-0-387-70984-0>
41. Corradini MG, Peleg M (2009) Dynamic model of heat inactivation kinetics for bacterial adaptation. *Appl Environ Microbiol* 75(8):2590–2597. <https://doi.org/10.1128/aem.02167-08>
42. Guescini M, Sisti D, Rocchi MBL, Panebianco R, Tibollo P, Stocchi V (2013) Accurate and precise DNA quantification in the presence of different amplification efficiencies using an improved *Cy0* method. *PLoS ONE* 8(7):e68481
43. Hansford GS (1997) Chapter 8. Recent developments in modeling the kinetics of bioleaching. In: Rawlings DE (ed) *Biomining: theory, microbes and industrial processes*. Springer, Berlin, pp 153–175. https://doi.org/10.1007/978-3-662-06111-4_8
44. Hansford GS, Bailey AD (1992) The logistic equation for modelling bacterial oxidation kinetics. *Miner Eng* 5(10):1355–1364. [https://doi.org/10.1016/0892-6875\(92\)90171-5](https://doi.org/10.1016/0892-6875(92)90171-5)
45. Hansford GS, Miller DM (1993) Biooxidation of a gold-bearing pyrite-arsenopyrite concentrate. *FEMS Microbiol Rev* 11(1):175–181
46. Mazaheri D, Shojaosadati SA (2013) Mathematical models for microbial kinetics in solid-state fermentation: a review. *Iran J Biotechnol* 11(3):156–167. <https://doi.org/10.5812/ijb.9426>
47. Miller DM, Hansford GS (1992) The use of the logistic equation for modelling the performance of a biooxidation pilot plant treating a gold-bearing arsenopyrite-pyrite concentrate. *Miner Eng* 5(7):737–749. [https://doi.org/10.1016/0892-6875\(92\)90243-3](https://doi.org/10.1016/0892-6875(92)90243-3)
48. Murray JD (2002) *Mathematical biology I. An Introduction*, 3rd edn. Springer-Verlag, New York
49. Rutledge RG, Stewart D (2008) A kinetic-based sigmoidal model for the polymerase chain reaction and its application to high-capacity absolute quantitative real-time PCR. *BMC Biotechnol* 8(1):47. <https://doi.org/10.1186/1472-6750-8-47>

50. Dhanasekar R, Viruthagiri T (2005) Batch kinetics and modeling of poly-b-hydroxy butyrate synthesis from *Azotobacter vinelandii* using different carbon sources. *Indian J Chem Technol* 12:322–326
51. Villadsen J (2015) Chapter 7. Kinetics of bio-reactions. In: Villadsen J (ed) *Fundamental bioengineering*. Wiley, New York, pp 183–232. <https://doi.org/10.1002/9783527697441.ch07>
52. Tarrío-Saavedra J, López-Beceiro J, Naya S, Francisco-Fernández M, Artiaga R (2014) Simulation study for generalized logistic function in thermal data modeling. *J Therm Anal Calorim* 118(2):1253–1268. <https://doi.org/10.1007/s10973-014-3887-z>
53. Burnham AK (2017) Use and misuse of logistic equations for modeling chemical kinetics. *J Therm Anal Calorim* 127(1):1107–1116. <https://doi.org/10.1007/s10973-015-4879-3>
54. Niven RK (2006) q-Exponential structure of arbitrary-order reaction kinetics. *Chem Eng Sci* 61(11):3785–3790. <https://doi.org/10.1016/j.ces.2005.12.004>
55. Brown ME, Glass BD (1999) Pharmaceutical applications of the Prout–Tompkins rate equation. *Int J Pharm* 190(2):129–137. [https://doi.org/10.1016/S0378-5173\(99\)00292-6](https://doi.org/10.1016/S0378-5173(99)00292-6)
56. Jones CA, Kelly DP (1983) Growth of *Thiobacillus ferrooxidans* on ferrous iron in chemostat culture: influence of product and substrate inhibition. *J Chem Technol Biotechnol* 33(4):241–261. <https://doi.org/10.1002/jctb.280330407>

Publisher's Note Springer Nature remains neutral with regard to jurisdictional claims in published maps and institutional affiliations.